

DeDoDe: Detect, Don't Describe — Describe, Don't Detect for Local Feature Matching

Johan Edstedt¹ Georg Bökman² Mårten Wadenbäck¹ Michael Felsberg¹

¹Linköping University, ²Chalmers University of Technology

Abstract

Keypoint detection is a pivotal step in 3D reconstruction, whereby sets of (up to) K points are detected in each view of a scene. Crucially, the detected points need to be consistent between views, i.e., correspond to the same 3D point in the scene. One of the main challenges with keypoint detection is the formulation of the learning objective. Previous learning-based methods typically jointly learn descriptors with keypoints, and treat the keypoint detection as a binary classification task on mutual nearest neighbours. However, basing keypoint detection on descriptor nearest neighbours is a proxy task, which is not guaranteed to produce 3D-consistent keypoints. Furthermore, this ties the keypoints to a specific descriptor, complicating downstream usage. In this work, we instead learn keypoints directly from 3D consistency. To this end, we train the detector to detect tracks from large-scale SfM. As these points are often overly sparse, we derive a semi-supervised two-view detection objective to expand this set to a desired number of detections. To train a descriptor, we maximize the mutual nearest neighbour objective over the keypoints with a separate network. Results show that our approach, DeDoDe, achieves significant gains on multiple geometry benchmarks. Code is provided at github.com/Parskatt/DeDoDe.

1. Introduction

Incremental Structure from Motion (SfM) can roughly be divided into detection, matching, and estimation. In the detection stage, we seek to detect keypoints in the 3D scene that are consistent between views. This is a crucial step, as the optimization process relies on accurate 3D tracks, i.e., 3D points consistently detected in multiple views. While keypoints are necessary for SfM, it is difficult to formulate a learning-based objective. Traditional methods often rely on proxy tasks such as extrema in differences of Gaussians [19], corner detection [12], while learning-based methods often aim to detect mutual nearest neighbours of descriptors [10, 32]. While these methods can result in distinct and reproducible points, they do not directly opti-

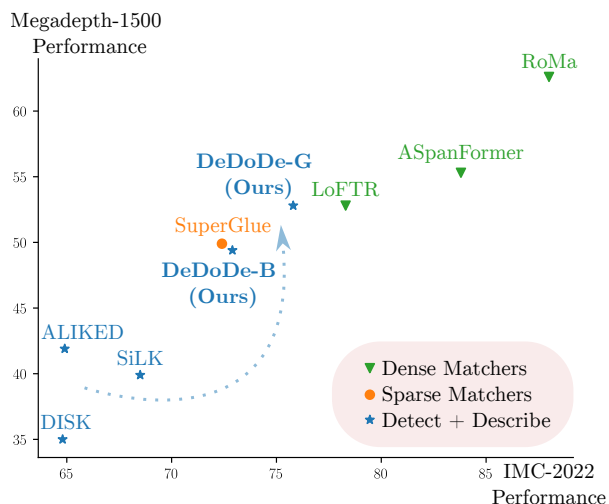


Figure 1. **DeDoDe closes the matching gap.** There is a large gap in performance between traditional detector/descriptor models and fully-fledged matching models. DeDoDe significantly reduces this gap, demonstrating the untapped potential of the simple detector+descriptor approach.

mize 3D consistency of the points between views. In order to tackle this discrepancy, we propose to directly learn 3D consistency by detecting 3D tracks. To do this we use SfM reconstructions directly as supervision. Since we have access to ground truth 3D tracks, we can directly optimize to detect these. However, as the 3D tracks are produced by a base detector, there is a risk of missing reliable keypoints discarded by the original detector. To mitigate this problem, we propose a semi-supervised two-view top- k consistency objective, which enables us to surpass the initial detector both in precision and recall. A detailed description of our approach is provided in Section 4.

When training detectors and descriptors jointly, the descriptor objective is complex. In contrast, we can directly optimize the mutual nearest neighbour negative log-likelihood for the descriptions over DeDoDe keypoints to train the DeDoDe descriptor, which we will refer to as DeDoDe-B. While this model performs well, local features



Figure 2. **Qualitative comparison.** **Left:** Matches from the joint detector/descriptor DISK [32], **Right:** Matches from our decoupled detector/descriptor DeDoDe. DeDoDe shows substantial improvements in both detector precision and descriptor quality in comparison to previous approaches, performing well even under significant changes in viewpoint.

struggle with describing repeating structures, which requires a larger context. Recent work [9] has shown promising results of using globally informed DINOv2 [22] features for dense matching. We show that incorporating frozen DINOv2 features into a larger version of our descriptor, which we call DeDoDe-G, also increases performance. Our approach to descriptor learning is detailed in Section 5.

Finally, we perform an extensive set of SotA experiments and ablations in Section 6, in which we find that DeDoDe sets a new state-of-the-art in feature matching. Our approach bridges the gap between the traditional detector+descriptor approach to matching and modern end-to-end matchers as can be seen in Figure 1. A qualitative comparison between the joint detector/descriptor DISK [32] and DeDoDe is presented in Figure 2.

2. Related Work

Keypoint Detection from Descriptors: Dusmanu et al. [7] proposed a joint descriptor/detector pipeline. Revaud et al. [25] extended these ideas and proposed a set of auxiliary losses to improve the detector. Tyszkiewicz et al. [32] proposed DISK, which uses a joint training objective for keypoint detection and description through policy gradient optimization, enabling backpropagation to the detector. Zhao et al. [38, 39] proposed ALIKE and ALIKED, where a local softmax weighting approach is used for keypoint detection that enables backpropagation to the detector.

Keypoint Detection from a Base Detector: Closest to our work are keypoint detectors that aim to surpass a base detector. One of the earliest works TaSK [28] classified keypoints that are consistent over long time periods, an idea that was further improved in TILDE [33]. A similar approach was investigated by Hartmann et al. [13], where a classifier was trained to discriminate SfM matchable keypoints. LIFT [36] crops small patches around SfM tracks, but does not optimize for detecting tracks directly. SuperPoint [6] is trained from an initial base detector by means of a synthetic training set of corners. A second detector is then trained to produce consistent detections of the base detector for heavily augmented images. More recent approaches, such as

SOLD² [23] and DeepLSD [24] further develop these ideas for line detection. Our work can be seen as further development of these ideas with some key differences. In contrast to previous work we introduce a top- k two-view semi-supervised detection objective combined with a coverage objective. Furthermore, we use an aligned but decoupled detector/descriptor learning approach. See Section 4.

Whether to Couple or Decouple Keypoint Detection and Description:

Traditionally, handcrafted feature detection pipelines, *e.g.* SIFT [19], the keypoint detection is independent of the descriptors. Early learned work in a similar fashion followed the decoupled approach [2, 20, 21]. However, this approach has been called into question in later works [7, 27, 30], with the reasoning that descriptors often succeed in matching where keypoints fail. Hence most following work has worked in the joint learning setting [10, 25, 32], which binds the keypoints to a specific descriptor. Recently, Li et al. [16], argue that the joint training is detrimental, as poor descriptors lead to unreliable mutual nearest neighbours, resulting in worse keypoint detectors. However, they still use the descriptor features as input to the detector network. In contrast to joint previous works, we consider an aligned objective that is still decoupled.

3. Why Decouple Keypoint Detection and Description?

In this paper we argue for a descriptor-agnostic approach to keypoint detection, see Figure 3. There are multiple reasons for this, we summarize the main points below

1. **Compatibility:** Mutual nearest neighbours of a certain descriptor does not guarantee general matchability or consistency. By being agnostic to the descriptor, our keypoints can be used for arbitrary matchers, as we demonstrate in Table 1.
2. **Decoupling Gains:** Thinking in a modular fashion lets us design decoupled experiments, for example Table 2 and 3, as well as Table 6.
3. **Performance:** Our approach improves significantly on the state-of-the-art, see Figure 1. This demonstrates the soundness of our approach.

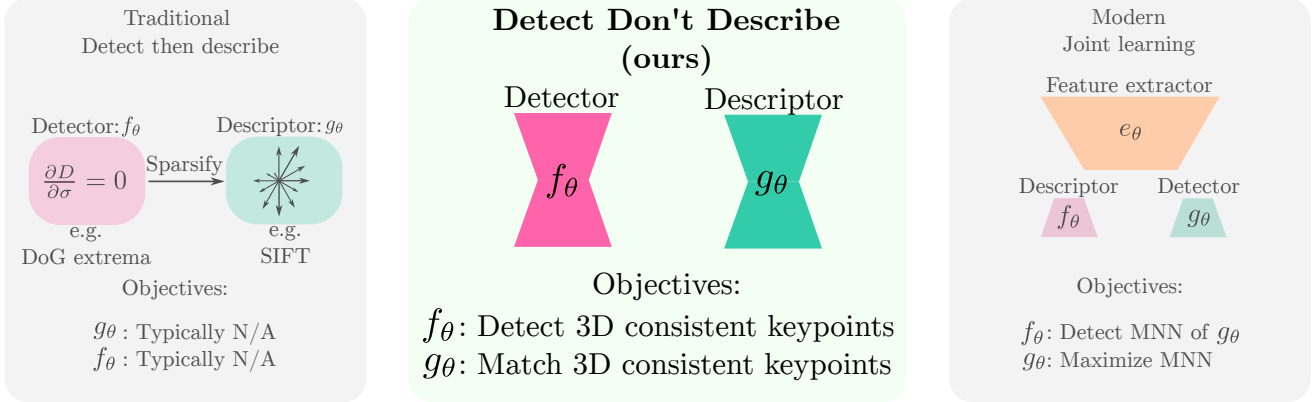


Figure 3. **Previous detector/descriptor approaches compared to DeDoDe.** **Left:** Traditional methods are typically two-stage, first detecting promising keypoints with a detector f_θ , which are subsequently described by a descriptor g_θ . This approach suffers from the lack of synergy between the detector and descriptor [7, 30]. **Right:** Later, learning-based methods using the joint learning paradigm were introduced. Here the objectives of the descriptor and the detector are aligned. However, this has other issues. One issue is that introducing inter-dependencies of the descriptor/detector often degrades performance [16]. For example, repeating complex patterns may constitute excellent keypoints, but fail to match, while unique textureless regions may match, but do not produce exact localization. **Middle:** In this paper we take a new approach and decouple the descriptor and detector learning while having aligned objectives. We do this by learning to detect and match 3D tracks from large-scale SfM. In Section 4 we describe how we create a training objective for the detector, and in Section 5 we describe the approach for the descriptor. Our approach leads to significant improvements to the state-of-the-art, as demonstrated in Section 6, showing the potential of detector based methods.

The following sections describe our method. In Section 4 we introduce the DeDoDe detector, and in Section 5 the DeDoDe descriptor.

4. Detect, Don’t Describe

For an overview of our approach, see Figure 4.

4.1. Preliminaries

Let $f_\theta(x|I)$ be a mapping producing a log density (possibly non-normalized) over an image I . We would like this network to produce high values for all 3D consistent keypoints, and low values otherwise. Now let

$$\mathcal{D} = \{I^j\}_{j=1}^J \quad (1)$$

be a dataset of images with cardinality $|\mathcal{D}| = J$. We will denote the set of keypoints for a given image I^j in pixel coordinates as $\mathbf{x}_{\text{kp}}^j = \{x_i^j\}_{i=1}^{K^j}$ where K^j is the number of observable keypoints in image I^j . Formally, we want to maximize the following log-likelihood objective,

$$\max_{\theta} \sum_{j=1}^{|\mathcal{D}|} \sum_{i=1}^{K^j} f_\theta(x_i^j|I^j) - \log Z_\theta(I^j), \quad (2)$$

where we have defined

$$Z_\theta(I^j) := \sum_{x^j \in I^j} \exp(f_\theta(x^j|I^j)).^1 \quad (3)$$

¹The notation $x^j \in I^j$ here means normalization over all pixel coordinates in image I^j .

That is, we want to maximize the likelihood of sampling 3D keypoints. For notational convenience, we will also define

$$p_{f_\theta}(x_i^j) := \exp(f_\theta(x_i^j|I^j) - \log Z_\theta(I^j)) \quad (4)$$

The main challenge of keypoint detection is how to maximize Equation 2. In particular, in contrast to other keypoint tasks, there are no ground truth annotations. In this paper we will consider a good prior for a keypoint as a 2D detection (from a base keypoint detector) that has “survived” 3D reconstruction, *i.e.*, formed a 3D track.

4.2. Keypoints as 3D Tracks

We use a dataset of large-scale SfM reconstructions, MegaDepth [17], where SIFT [19] is used as keypoint detector, *i.e.*, scale space extrema. These detections go through a filtering process, whereby only 3D consistent detections remains after optimization finishes. However, in each image, only a fraction of all visible tracks are detected. To solve this issue we propose to sample pairs of images I^A and I^B , and use the union of covisible detections. We obtain the covisibility by means of Multi-View Stereo depth maps.

4.3. A Smooth Keypoint Detection Prior

Due to the detector producing detections on a discrete grid, and for reasons we will discuss in Section 4.4, a smooth detection prior is desirable. We do this by a 2-stage process. For both I^A and I^B we start by placing Dirac deltas $\delta(\mathbf{x}_{\text{kp}})$

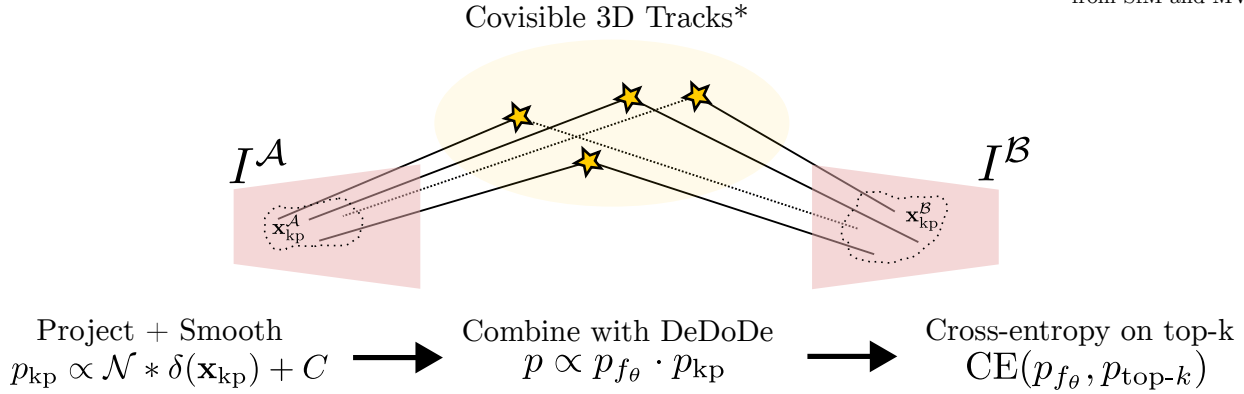


Figure 4. **Training objective of DeDoDe for keypoint detection.** We sample an image pair from a large-scale SfM + MVS reconstruction. (i) For this pair we find all covisible detections (from a base detector) that resulted in a 3D track. We take the union of tracks detected in the image (indicated by filled lines in the figure), and tracks not detected but covisible (indicated by dotted lines in the figure). See Section 4.2. (ii) We project these detections into the images. We then convert this point set into a softened distribution, which constitutes our prior for good keypoints, see Section 4.3. (iii) We then condition this distribution with the predictions of DeDoDe, as the base detector may have false negatives, see Section 4.4. (iv) Finally, we threshold this distribution at the k :th highest value, and compute the cross-entropy between DeDoDe and the target. Using top- k stabilizes the self-supervised objective. See Section 4.5.

at the nearest grid position of the detections. We then convolve these with a Gaussian kernel with $\sigma = 0.5$ pixels, and add a small constant that corresponds to a uniform distribution. Mathematically,

$$\tilde{p}_{kp}^A \propto \mathcal{N}(0, \sigma^2) * \delta(\mathbf{x}_{kp}^A) + C^A, \quad (5)$$

$$\tilde{p}_{kp}^B \propto \mathcal{N}(0, \sigma^2) * \delta(\mathbf{x}_{kp}^B) + C^B. \quad (6)$$

Finally we warp the distributions of \mathcal{A}, \mathcal{B} using the depth to produce $\tilde{p}_{kp}^{A \rightarrow B}, \tilde{p}_{kp}^{B \rightarrow A}$. Combining yields

$$p_{kp}^A \propto \tilde{p}_{kp}^A \cdot \tilde{p}_{kp}^{B \rightarrow A}, \quad (7)$$

$$p_{kp}^B \propto \tilde{p}_{kp}^B \cdot \tilde{p}_{kp}^{A \rightarrow B}. \quad (8)$$

In practice, the constants in equations 5 and 6 are implicitly defined by approximating $\log p_{kp} \approx \vartheta p_{kp}$, with $\vartheta = 50$. The end result is a detection prior which produces particularly high values at 3D-tracks detected in *both* images, which we found beneficial.

Note that while this is a simple and powerful way of producing a detection prior, there is a multitude of ways one could construct it. For example, we could exclude all tracks smaller than a certain track length, or only include tracks with sufficiently small reprojection errors. However, such approaches introduce more complex hyperparameters, and we found our simple approach to already yield state-of-the-art results.

4.4. Posterior Detection Distribution

While the detection prior yields good detections, we found that it is often overly sparse in practice. This is due to the

base detector not detecting all keypoints, *i.e.*, insufficient recall. To amend this issue, we propose to update the prior distribution with the predictions of f_θ , *i.e.*,

$$p \propto p_{f_\theta} \cdot p_{kp}. \quad (9)$$

This enables the network to detect keypoints missed by the base detector. Note that while it would appear that multiplying the distributions cannot add detections, the fact that we have put a small flat prior on the keypoint distribution in practice creates peaks around the model detections that enable detection of additional keypoints.

4.5. Detector Training Objective

In principle, one could form an objective directly using the cross entropy between p_{f_θ} and p . However, we found training to be more stable when thresholding and binarizing p in practice. This is due to the non-binary objective having degenerate solutions, as we show in Suppl. F. To this end, we select the top- k detections in a batch, where we empirically select $k = \text{batchsize} \cdot 1024$, to construct the target distributions. Then we simply compute the cross entropy between the predicted distribution and the target as a loss,

$$\mathcal{L}_{\text{detection}} = \text{CE}(p_{f_\theta}, p_{\text{top-}k}). \quad (10)$$

We additionally add a coverage regularization on f_θ by computing the cross-entropy between a low-pass filtered p_{f_θ} and a binary distribution p_{MVS} indicating successful MVS reconstruction, *i.e.*,

$$\mathcal{L}_{\text{coverage}} = \text{CE}(\mathcal{N}(0, \sigma^2) * p_{f_\theta}, \mathcal{N}(0, \sigma^2) * p_{\text{MVS}}). \quad (11)$$

In practice we used $\sigma = 12.5$ pixels. This regularization is necessary, as the network may otherwise produce detections in unmatchable regions (e.g. sky). Our combined loss is

$$\mathcal{L} = \mathcal{L}_{\text{detection}} + \mathcal{L}_{\text{coverage}}. \quad (12)$$

As with our choice of prior distribution, these choices are not guaranteed to be optimal, but worked well in practice. Note that the choice of k depends on the expected overlap between the views. For difficult pairs, one would expect fewer keypoints to overlap. It is in principle possible to control the sparsity of the detector by decreasing or increasing k , but investigation of this is outside the scope of the paper.

4.6. Sampling Keypoints at Inference

To sample keypoints, we follow previous work and select the top K most likely keypoints from f_θ . We follow SiLK [10] and do not employ non-max suppression.

4.7. Network Architecture

Encoder: We use a VGG-19 network pretrained on ImageNet, implemented in `torchvision`. We use strides [1, 2, 4, 8]. The output at each scale is a feature-map with [64, 128, 256, 512] channels respectively.

Decoder: We use the architecture of the depthwise convolution refiners proposed in DKM [8], with 8 blocks per scale and internal dimension [64, 128, 256, 512]. The input at each scale is the encoded features, as well as context from previous decoding layers. The output at each scale is a residual addition to a dense grid of keypoint logits. Between each scale these logits are upsampled using bicubic interpolation.

Note that our network is different from DKM which takes two images as input, constructing a local correlation volume + stacked feature maps, while ours simply refines the features.

5. Describe, Don’t Detect

5.1. Descriptor Preliminaries

Given two sets of keypoints, $\mathbf{x}_{\text{kp}}^A, \mathbf{x}_{\text{kp}}^B$, and the respective images I^A, I^B , the task of a descriptor network $\mathbf{g}_\theta(x|I^A)$ is to produce descriptions $\mathbf{g}_\theta(\mathbf{x}_{\text{kp}}^A|I^A), \mathbf{g}_\theta(\mathbf{x}_{\text{kp}}^B|I^B)$ that match well for keypoints corresponding to the same 3D point, and match poorly for non-corresponding keypoints.

We choose the probabilistic framework, as is common [10, 32], where

$$p_{\mathbf{g}_\theta}(x^A|x^B) := \frac{\exp(\langle \mathbf{g}_\theta(x^A|I^A), \mathbf{g}_\theta(x^B|I^B) \rangle)}{\sum_{x_i^A \in \mathbf{x}_{\text{kp}}^A} \exp(\langle \mathbf{g}_\theta(x_i^A|I^A), \mathbf{g}_\theta(x^B|I^B) \rangle)}, \quad (13)$$

defines the conditional matching distribution, and formally define matching likelihoods as

$$L_{\mathbf{g}_\theta}(x^A, x^B) := p_{\mathbf{g}_\theta}(x^B|x^B) \cdot p_{\mathbf{g}_\theta}(x^B|x^A). \quad (14)$$

This objective has the benefit of working well with mutual nearest neighbours based downstream matchers.

5.2. Descriptor Training Objective

Taking the logarithm of equation (14) leads to a straightforward log-likelihood objective

$$\ell_{\mathbf{g}_\theta}(x^A, x^B) = \log p_{\mathbf{g}_\theta}(x^A|x^B) + \log p_{\mathbf{g}_\theta}(x^B|x^A). \quad (15)$$

The main difficulty with optimizing this objective is the normalizing term, which in most works is either approximated [32], or brute-force optimized in lower resolution [10]. However, as our formulation is decoupled, we face no such issues and simply use trained DeDoDe keypoints. During training, similarly to inference, we sample $K = 5000$ descriptions from a dense grid, using a pretrained DeDoDe detector.

5.3. Descriptor Network Architecture

The architecture of the descriptor largely matches that of the detector. Importantly, however, they do not share any weights.

Encoder: We use a VGG-19 network pretrained on ImageNet, implemented in `torchvision`. We use features at strides [1, 2, 4, 8]. The output at each scale is a feature-map with [64, 128, 256, 512] channels respectively.

Decoder: We use the architecture of the depthwise convolution refiners proposed in DKM [8], with 5 blocks per scale and internal dimension [32, 64, 256, 512]. We call this model DeDoDe-B. The input at each stride is the encoded features, as well as context from previous decoding layers. The output at each scale is a residual addition to a dense grid of descriptions. Between each scale the descriptions are upsampled using bilinear interpolation. We use a description dimension of 256. We normalize the descriptions, and use a temperature of 20^{-1} during both training and inference.

Note, as for the detector, that our network is different from DKM which takes two images as input, constructing a local correlation volume + stacked feature maps, while ours simply refines the features of one image.

DeDoDe-G: To explore the full potential of detector descriptor methods, we propose to incorporate features from DINOv2 [22]. This addition is simple in our framework, we just add frozen DINOv2 features at stride 14, with a corresponding decoder stage. We use an internal dimension of 768 for this decoder. With this simple addition, we achieve impressive performance gains as demonstrated in Table 1 and Table 4.

6. Experiments

6.1. Training

DeDoDe Detector: We train for 100,000 steps of batch size 8 on the MegaDepth dataset, using the same training split as DKM [8]. We use a fixed image size of 512×512 . Training is done on a single A100 GPU, and takes about 30 hours.

DeDoDe Descriptor: Mirroring our detector training setup, we train for 100,000 steps of batch size 8 on the MegaDepth dataset. We use a single A100 GPU, and training takes about 24 hours. The slightly shorter training time comes from using fewer blocks in the decoder.

6.2. Inference

For all SotA experiments we run at a resolution of 784×784 and sample top- k keypoints.

6.3. Integrating DeDoDe With Matchers

Recent works [8, 29] often claim that detection localization errors hinder performance. To investigate this claim, we integrate DeDoDe into the recent SotA matcher RoMa [9]. We integrate RoMa into our detection framework by sampling the dense warp of RoMa at the location of DeDoDe keypoints, and match each keypoint by warping it to the other image and finding its nearest-neighbour DeDoDe keypoint there.

As expected, quantizing the RoMa warp to DeDoDe keypoints decreases performance compared to the results of RoMa, but increases the results compared to our detector+descriptor approach. If we view RoMa as an oracle, we can view the detector gap as about 7 points AUC@5°. This indicates that there are still significant gains that can be made by improving the detector further.

6.4. Qualitative Examples

DeDoDe Keypoints: Here we qualitatively demonstrate the types of keypoints and matches learned by DeDoDe. In Figure 5 we show DeDoDe matches on a non-cherrypicked, *i.e.* randomly chosen, pair from the MegaDepth-1500 test-set. We find that DeDoDe produces repeatable keypoints that match well.

6.5. SotA Comparison

MegaDepth-1500 Relative Pose: MegaDepth-1500 is a relative pose benchmark proposed in LoFTR [29], and consists of 1500 pairs of images in two scenes of the MegaDepth dataset, which are non-overlapping with our training set. We compare DeDoDe against previous detector/descriptor models, as well as fully fledged matchers. We present results in Table 1. Our results clearly show the soundness of our approach, with gains of +17.8 AUC@5°

Table 1. **SotA comparison on the Megadepth-1500 benchmark.** The top portion contains dense and detector free matching methods, the middle part keypoint matching methods, while the bottom portion contains traditional MNN matching from keypoints and descriptors. Measured in AUC (higher is better).

Method ↓	AUC →	@5°	@10°	@20°
LoFTR [29] CVPR'21		52.8	69.2	81.2
SE2-LoFTR-4 [3] CVPRW'22		52.6	69.2	81.4
QuadTree [31] ICLR'22		54.6	70.5	82.2
ASpanFormer [5] ECCV'22		55.3	71.5	83.1
ASTR [37] CVPR'23		58.4	73.1	83.8
DKM [8] CVPR'23		60.4	74.9	85.1
PMatch [40] CVPR'23		61.4	75.7	85.7
RoMa [9] Arxiv'23		62.6	76.7	86.3
DeDoDe + RoMa		55.1	71.6	83.5
SuperGlue [26] CVPR'19		49.7	67.1	80.0
SGMNet [4] CVPR'21		43.2	61.6	75.6
LightGlue [18] ICCV'23		49.9	67.0	80.1
SuperPoint [6] CVPRW'18		31.7	46.8	60.1
DISK [32] Neurips'20		35.0	51.4	64.9
ALIKED [39] TIM'23		41.9	58.4	71.7
SiLK [10] ICCV'23		39.9	55.1	66.9
DeDoDe-B		49.4	65.5	77.7
DeDoDe-G		52.8	69.7	82.0

Table 2. **SotA comparison on MegaDepth-Repeatability-10k.** *:Non-max suppression removed. Note that DeDoDe and SiLK do not use non-max suppression.

Method	Repeatability @ 10k		
	0.1%	0.2%	0.5%
DISK [32] Neurips'20	18.4	56.6	93.0
DISK* [32] Neurips'20	32.6	60.0	83.9
ALIKED [39] IEEE-TIM'23	19.4	63.3	90.8
ALIKED* [39] IEEE-TIM'23	26.4	63.2	85.6
SiLK [10] ICCV'23	21.2	46.5	67.1
DeDoDe	40.1	63.7	80.3

compared to DISK, +12.9 AUC@5° compared to SiLK, and +10.9 AUC@5° compared to ALIKED.

MegaDepth Detector Repeatability: Previous benchmarks for keypoint detectors often jointly measure the repeatability of keypoints and the matchability of the descriptors into single metrics. Here we aim to disentangle these two measurements, and *only* measure keypoint repeatability. To do this, we use the ground truth warp, and measure the percentage of inliers, *i.e.*, pairs of keypoints close enough, under a set of thresholds. We investigate two different settings, the many keypoints setting (maximum 10000 keypoints), and the few keypoint setting (maximum 2000 keypoints). Results are presented in Table 2 and Table 3. The results reveal interesting properties of

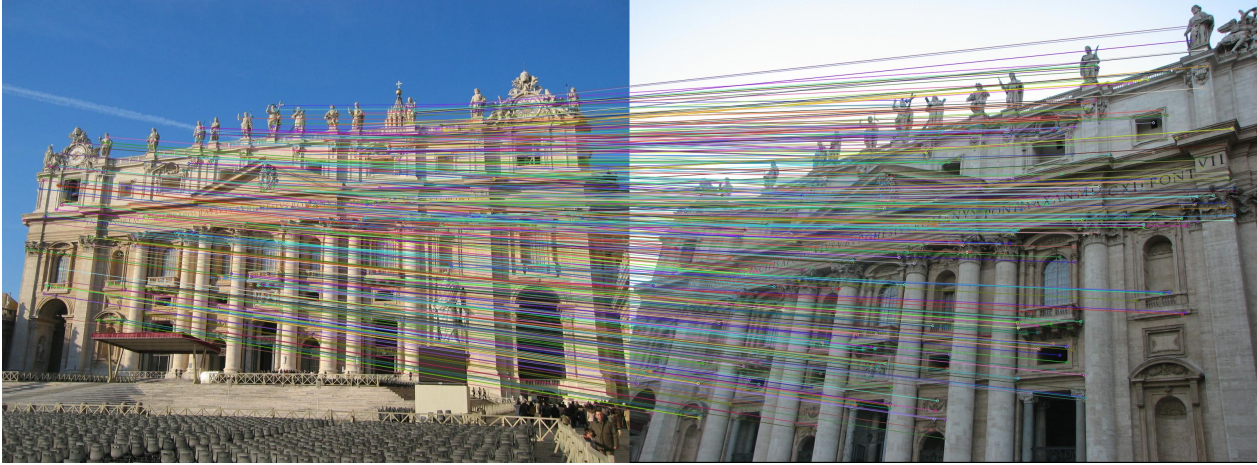


Figure 5. **Qualitative example of DeDoDe matches.** We picked a random pair in the MegaDepth-1500 testset and visualize confident DeDoDe matches. As can be seen in the figure, DeDoDe produces reliable keypoints and good matches, even in challenging situations. There are still outliers however, particularly for repeating structures such as similar statues, and identical pillars. Best viewed in high resolution.

Table 3. **SotA comparison on MegaDepth-Repeatability-2k.** *: Non-max suppression removed. Note that DeDoDe and SiLK do not use non-max suppression.

Method	Repeatability @ 2k		
	@0.1%	@0.2%	@0.5%
DISK [32] <small>Neurips'20</small>	17.0	41.1	65.7
DISK* [32] <small>Neurips'20</small>	21.8	40.1	57.5
SiLK [10] <small>ICCV'23</small>	8.2	21.8	35.8
ALIKED [39] <small>IEEE-TIM'23</small>	19.3	45.4	67.9
ALIKED* [39] <small>IEEE-TIM'23</small>	21.2	46.1	66.5
DeDoDe	24.3	41.8	58.3

detectors. In particular, we find that DeDoDe and SiLK show large gains from higher numbers of keypoints for tight thresholds, while DISK shows large gains in loose thresholds. This indicates that DISK detections consists of a small number of certain detections, with a large number of uncertain detections, whereas DeDoDe and SiLK detections contain a larger spectrum. This might be due to the training of DISK, which is regularized to have single detections in patches by local softmax [32], while DeDoDe and SiLK do not. It can also be observed that ALIKED shows very minor gains from increasing the number of keypoints. This indicates that ALIKED may be better suited for usecases where very few but reliable keypoints are required, while DeDoDe scales better for larger numbers. Finally, note that while DeDoDe, ALIKED, and DISK are trained on the MegaDepth dataset, SiLK is trained only using synthetic homographies.

Image Matching Challenge 2022: The Image Matching Challenge 2022 [14] is composed of challenging un-

calibrated relative pose estimation pairs. Different from MegaDepth-1500, the test set is hidden and does not derive from MegaDepth, and may therefore better indicate generalization performance, especially for models such as DeDoDe that train on MegaDepth. We follow the setup in SiLK [10] and use 30,000 keypoints, and MAGSAC++ [1] with a threshold of 0.25 pixels. We use a fixed image size of 784×784 . We follow the approach in RoMa [9] and report results on the hidden test set. We present results in Table 4. Here too, DeDoDe achieves significant improvements to the state-of-the-art, with results competitive with the graph neural network (GNN) matcher SuperGlue [26], and surpassing the recent SiLK [10] with +7.4 points mAA.

6.6. Ablation Study

Design Decisions: Here we investigate the impact of our design decisions. In Setting I, we supervise directly using the detection prior in Section 4.3. This decreases performance, in particular for coarse thresholds. In Setting II we do not include the coverage term introduced in Section 4.5. This decreases performance across all thresholds. We attribute this to the network not learning to attenuate certainty in unmatchable regions, *e.g.*, sky.

Exchanging Components with Previous Methods: In this section we compare the effect of the detector and descriptor of DeDoDe by exchanging components of SIFT, DISK, and DeDoDe. We present results in Table 6. Interestingly, using SIFT detections with DeDoDe descriptions outperforms the DISK feature matcher. Similarly, replacing the DISK descriptor with DeDoDe also improves performance. Note however that while results are improved com-

Table 4. **SotA comparison on the IMC2022 benchmark.** Relative pose estimation results on the IMC2022 [14] hidden test set, measured in mAA (higher is better). The top portion contains dense and detector free matching methods, the middle part key-point matching methods, while the bottom portion contains traditional MNN matching from keypoints and descriptors.

Method ↓	mAA →	@10
LoFTR [29] <small>CVPR'21</small>		78.3
MatchFormer [34] <small>ACCV'22</small>		78.3
QuadTree [31] <small>ICLR'22</small>		81.7
ASpanFormer [5] <small>ECCV'22</small>		83.8
RoMa [9] <small>Arxiv'23</small>		88.0
<hr/>		
SP [6]+SuperGlue [26]		72.4
<hr/>		
DISK [32] <small>Neurips'20</small>		64.8
ALIKED [39] <small>IEEE-TIM'23</small>		64.9
SiLK [10] <small>ICCV'23</small>		68.5
DeDoDe-B		72.9
DeDoDe-G		75.8

Table 5. **Ablation study on MegaDepth-Repeatability-10k.** We investigate the performance effect of two of our contributions on the detector repeatability using a fixed resolution of 512×512 .

Method	Repeatability @ 10k		
	0.1%	0.2%	0.5%
I: Prior Distribution as Target	34.8	61.3	78.0
II: No Coverage Loss	29.7	59.4	78.0
DeDoDe (512x512)	37.1	68.1	84.8

pared to the original methods with DeDoDe descriptor, it is a significant decrease compared to when using DeDoDe detections, with an absolute decrease of 8 points AUC.

Replacing the detector in DISK with DeDoDe slightly decreases the performance. We attribute this to the training of DISK, which learns keypoints that is likely to be mutual nearest neighbours of the descriptor. SIFT descriptors, in contrast to DISK, require scale and rotation estimation from the keypoint. To circumvent this issue we sample SIFT keypoints within a distance of 1 pixel from DeDoDe keypoints. Note that this is a inferior version to our original detector as it results in a subset of the original SIFT keypoints. It is therefore not surprising that results are slightly degraded.

7. Conclusion

We have presented DeDoDe, a descriptor-agnostic modular approach to geometric keypoint detection. We did this by formulating keypoint detection as detecting points that have successfully created 3D tracks in large-scale SfM. We introduced a two-view objective, in order to reduce the sparseness of the detections, and furthermore proposed a suitable descriptor objective. Our experiments show that

Table 6. **Ablation study on the Megadepth-1500 benchmark.** Here we ablate the gains from incorporating the DeDoDe detector and descriptor to matching. As baselines we compare to using SIFT, or DISK [32]. *: SIFT requires scale and orientation estimation from the keypoints, see text for details.

Detector/Descriptor ↓	AUC →	@5°	@10°	@20°
SIFT/SIFT [19]		36.5	50.2	62.7
DISK/DISK [32] <small>Neurips'20</small>		35.0	51.4	64.9
DeDoDe/DeDoDe-B		49.4	65.5	77.7
<hr/>				
SIFT/DeDoDe-B		41.1	56.8	69.8
DISK/DeDoDe-B		41.5	57.9	71.0
<hr/>				
DeDoDe/SIFT*		34.1	49.1	62.0
DeDoDe/DISK		33.1	48.9	61.7

DeDoDe significantly improves on the state-of-the-art. DeDoDe enables a new research direction towards a modular detection and matching framework.

Limitations:

1. DeDoDe is dependent on the base detector. This means that potential stable keypoints can be missed. We remedied this by introducing a top- k semi-supervised objective during training.
2. DeDoDe is not trained with augmentations, contrary to common practice [10, 18]. It is possible that appropriate augmentation would increase the performance/generalization of our method.
3. DeDoDe tends to produce a large number of potential keypoints. In the few-keypoint setting this means that the repeatability degrades, as many keypoints are missed. Adjusting the hyperparameters of the keypoint target distribution may be able to address these issues.
4. The DeDoDe detector produces only keypoint locations, and does not estimate orientation/scale. This could potentially be remedied by using a separate network for estimating the local frame [15, 21, 35], although this would come at an additional computational cost.

Acknowledgements: We thank the reviewers for the constructive feedback that helped improve the paper. We thank Emanuel Sanchez Aimar and Ioannis Athanasiadis for the early discussions. This work was supported by the Wallenberg Artificial Intelligence, Autonomous Systems and Software Program (WASP), funded by Knut and Alice Wallenberg Foundation; and by the strategic research environment ELLIIT funded by the Swedish government. The computational resources were provided by the National Academic Infrastructure for Supercomputing in Sweden (NAISS) at C3SE partially funded by the Swedish Research Council through grant agreement no. 2022-06725, and by the Berzelius resource, provided by the Knut and Alice Wallenberg Foundation at the National Supercomputer Centre.

References

- [1] Daniel Barath, Jana Noskova, Maksym Ivashechkin, and Jiri Matas. Magsac++, a fast, reliable and accurate robust estimator. In *Proceedings of the IEEE/CVF conference on computer vision and pattern recognition*, pages 1304–1312, 2020. **7**
- [2] Axel Barroso-Laguna, Edgar Riba, Daniel Ponsa, and Krystian Mikolajczyk. Key. net: Keypoint detection by hand-crafted and learned cnn filters. In *Proceedings of the IEEE/CVF international conference on computer vision*, pages 5836–5844, 2019. **2**
- [3] Georg Bökman and Fredrik Kahl. A case for using rotation invariant features in state of the art feature matchers. In *Proceedings of the IEEE/CVF Conference on Computer Vision and Pattern Recognition*, pages 5110–5119, 2022. **6**
- [4] Hongkai Chen, Zixin Luo, Jiahui Zhang, Lei Zhou, Xuyang Bai, Zeyu Hu, Chiew-Lan Tai, and Long Quan. Learning to match features with seeded graph matching network. In *Proceedings of the IEEE/CVF International Conference on Computer Vision*, pages 6301–6310, 2021. **6**
- [5] Hongkai Chen, Zixin Luo, Lei Zhou, Yurun Tian, Mingmin Zhen, Tian Fang, David Mckinnon, Yanghai Tsin, and Long Quan. ASpanFormer: Detector-Free Image Matching with Adaptive Span Transformer. In *Proc. European Conference on Computer Vision (ECCV)*, 2022. **6, 8**
- [6] Daniel DeTone, Tomasz Malisiewicz, and Andrew Rabinovich. Superpoint: Self-supervised interest point detection and description. In *Proceedings of the IEEE conference on computer vision and pattern recognition workshops*, pages 224–236, 2018. **2, 6, 8**
- [7] Mihai Dusmanu, Ignacio Rocco, Tomas Pajdla, Marc Pollefeys, Josef Sivic, Akihiko Torii, and Torsten Sattler. D2-Net: A Trainable CNN for Joint Detection and Description of Local Features. In *Proceedings of the 2019 IEEE/CVF Conference on Computer Vision and Pattern Recognition*, 2019. **2, 3**
- [8] Johan Edstedt, Ioannis Athanasiadis, Mårten Wadenbäck, and Michael Felsberg. DKM: Dense Kernelized Feature Matching for Geometry Estimation. In *Proceedings of the IEEE Conference on Computer Vision and Pattern Recognition (CVPR)*, pages 17765–17775, 2023. **5, 6, 11**
- [9] Johan Edstedt, Qiyu Sun, Georg Bökman, Mårten Wadenbäck, and Michael Felsberg. RoMa: Revisiting robust losses for dense feature matching. *arXiv preprint arXiv:2305.15404*, 2023. **2, 6, 7, 8**
- [10] Pierre Gleize, Weiyao Wang, and Matt Feiszli. SiLK: Simple Learned Keypoints. In *Proceedings of the International Conference on Computer Vision (ICCV)*, 2023. **1, 2, 5, 6, 7, 8**
- [11] Jean-Bastien Grill, Florian Strub, Florent Althé, Corentin Tallec, Pierre Richemond, Elena Buchatskaya, Carl Doersch, Bernardo Avila Pires, Zhaohan Guo, Mohammad Gheshlaghi Azar, et al. Bootstrap your own latent—a new approach to self-supervised learning. *Advances in neural information processing systems*, 33:21271–21284, 2020. **12**
- [12] Chris Harris, Mike Stephens, et al. A combined corner and edge detector. In *Proceedings of the Alvey vision conference*, page 147–151, 1988. **1**
- [13] Wilfried Hartmann, Michal Havlena, and Konrad Schindler. Predicting matchability. In *Proceedings of the IEEE conference on computer vision and pattern recognition*, pages 9–16, 2014. **2**
- [14] Addison Howard, Eduard Trulls, etru1927, Kwang Moo Yi, old ufo, Sohier Dane, and Yuhe Jin. Image matching challenge 2022, 2022. **7, 8**
- [15] Jongmin Lee, Yoonwoo Jeong, and Minsu Cho. Self-supervised learning of image scale and orientation. In *31st British Machine Vision Conference 2021, BMVC 2021, Virtual Event, UK*. BMVA Press, 2021. **8**
- [16] Kunhong Li, Longguang Wang, Li Liu, Qing Ran, Kai Xu, and Yulan Guo. Decoupling makes weakly supervised local feature better. In *Proceedings of the IEEE/CVF Conference on Computer Vision and Pattern Recognition*, pages 15838–15848, 2022. **2, 3**
- [17] Zhengqi Li and Noah Snavely. Megadepth: Learning single-view depth prediction from internet photos. In *Proceedings of the IEEE Conference on Computer Vision and Pattern Recognition*, pages 2041–2050, 2018. **3**
- [18] Philipp Lindenberger, Paul-Edouard Sarlin, and Marc Pollefeys. LightGlue: Local Feature Matching at Light Speed. In *Proceedings of the International Conference on Computer Vision (ICCV)*, 2023. **6, 8**
- [19] David G Lowe. Distinctive image features from scale-invariant keypoints. *International journal of computer vision*, 60(2):91–110, 2004. **1, 2, 3, 8**
- [20] Anastasiia Mishchuk, Dmytro Mishkin, Filip Radenovic, and Jiri Matas. Working hard to know your neighbor’s margins: Local descriptor learning loss. *Advances in neural information processing systems*, 30, 2017. **2**
- [21] Dmytro Mishkin, Filip Radenovic, and Jiri Matas. Repeatability is not enough: Learning affine regions via discriminability. In *Proceedings of the European conference on computer vision (ECCV)*, pages 284–300, 2018. **2, 8**
- [22] Maxime Oquab, Timothée Darcet, Theo Moutakanni, Huy V. Vo, Marc Szafraniec, Vasil Khalidov, Pierre Fernandez, Daniel Haziza, Francisco Massa, Alaaeldin El-Nouby, Russell Howes, Po-Yao Huang, Hu Xu, Vasu Sharma, Shang-Wen Li, Wojciech Galuba, Mike Rabbat, Mido Assran, Nicolas Ballas, Gabriel Synnaeve, Ishan Misra, Herve Jegou, Julien Mairal, Patrick Labatut, Armand Joulin, and Piotr Bojanowski. DINOv2: Learning robust visual features without supervision. *arXiv:2304.07193*, 2023. **2, 5, 11, 12**
- [23] Rémi Pautrat, Juan-Ting Lin, Viktor Larsson, Martin R Oswald, and Marc Pollefeys. SOLD2: Self-supervised occlusion-aware line description and detection. In *Proceedings of the IEEE/CVF Conference on Computer Vision and Pattern Recognition*, pages 11368–11378, 2021. **2**
- [24] Rémi Pautrat, Daniel Barath, Viktor Larsson, Martin R Oswald, and Marc Pollefeys. DeepLSD: Line segment detection and refinement with deep image gradients. In *Proceedings of the IEEE/CVF Conference on Computer Vision and Pattern Recognition*, pages 17327–17336, 2023. **2**
- [25] Jerome Revaud, Cesar De Souza, Martin Humenberger, and Philippe Weinzaepfel. R2d2: Reliable and repeatable detector and descriptor. *Advances in neural information processing systems*, 32:12405–12415, 2019. **2**

- [26] Paul-Edouard Sarlin, Daniel DeTone, Tomasz Malisiewicz, and Andrew Rabinovich. Superglue: Learning feature matching with graph neural networks. In *Proceedings of the IEEE/CVF conference on computer vision and pattern recognition*, pages 4938–4947, 2020. 6, 7, 8
- [27] Torsten Sattler, Will Maddern, Carl Toft, Akihiko Torii, Lars Hammarstrand, Erik Stenborg, Daniel Safari, Masatoshi Okutomi, Marc Pollefeys, Josef Sivic, et al. Benchmarking 6dof outdoor visual localization in changing conditions. In *Proceedings of the IEEE Conference on Computer Vision and Pattern Recognition*, pages 8601–8610, 2018. 2
- [28] Christoph Strecha, Albrecht Lindner, Karim Ali, and Pascal Fua. Training for task specific keypoint detection. In *Pattern Recognition: 31st DAGM Symposium, Jena, Germany, September 9-11, 2009. Proceedings 31*, pages 151–160. Springer, 2009. 2
- [29] Jiaming Sun, Zehong Shen, Yuang Wang, Hujun Bao, and Xiaowei Zhou. LoFTR: Detector-free local feature matching with transformers. In *Proceedings of the IEEE/CVF Conference on Computer Vision and Pattern Recognition*, pages 8922–8931, 2021. 6, 8, 11
- [30] Hajime Taira, Masatoshi Okutomi, Torsten Sattler, Mircea Cimpoi, Marc Pollefeys, Josef Sivic, Tomas Pajdla, and Akihiko Torii. Inloc: Indoor visual localization with dense matching and view synthesis. In *Proceedings of the IEEE Conference on Computer Vision and Pattern Recognition*, pages 7199–7209, 2018. 2, 3
- [31] Shitao Tang, Jiahui Zhang, Siyu Zhu, and Ping Tan. Quadtree attention for vision transformers. In *International Conference on Learning Representations*, 2022. 6, 8
- [32] Michal J. Tyszkiewicz, Pascal Fua, and Eduard Trulls. DISK: learning local features with policy gradient. In *NeurIPS*, 2020. 1, 2, 5, 6, 7, 8, 11
- [33] Yannick Verdie, Kwang Yi, Pascal Fua, and Vincent Lepetit. Tilde: A temporally invariant learned detector. In *Proceedings of the IEEE conference on computer vision and pattern recognition*, pages 5279–5288, 2015. 2
- [34] Qing Wang, Jiaming Zhang, Kailun Yang, Kunyu Peng, and Rainer Stiefelhagen. MatchFormer: Interleaving attention in transformers for feature matching. In *Asian Conference on Computer Vision*, 2022. 8
- [35] Pei Yan, Yihua Tan, Shengzhou Xiong, Yuan Tai, and Yan-sheng Li. Learning soft estimator of keypoint scale and orientation with probabilistic covariant loss. In *Proceedings of the IEEE/CVF Conference on Computer Vision and Pattern Recognition*, pages 19406–19415, 2022. 8
- [36] Kwang Moo Yi, Eduard Trulls, Vincent Lepetit, and Pascal Fua. Lift: Learned invariant feature transform. In *European conference on computer vision*, pages 467–483. Springer, 2016. 2
- [37] Jiahuan Yu, Jiahao Chang, Jianfeng He, Tianzhu Zhang, Jiyang Yu, and Wu Feng. ASTR: Adaptive spot-guided transformer for consistent local feature matching. In *The IEEE/CVF Computer Vision and Pattern Recognition Conference (CVPR)*, 2023. 6
- [38] Xiaoming Zhao, Xingming Wu, Jinyu Miao, Weihai Chen, Peter CY Chen, and Zhengguo Li. Alike: Accurate and lightweight keypoint detection and descriptor extraction. *IEEE Transactions on Multimedia*, 2022. 2
- [39] Xiaoming Zhao, Xingming Wu, Weihai Chen, Peter C. Y. Chen, Qingsong Xu, and Zhengguo Li. Aliked: A lighter keypoint and descriptor extraction network via deformable transformation. *IEEE Transactions on Instrumentation & Measurement*, 72:1–16, 2023. 2, 6, 7, 8
- [40] Shengjie Zhu and Xiaoming Liu. PMatch: Paired masked image modeling for dense geometric matching. In *Proceedings of the IEEE/CVF Conference on Computer Vision and Pattern Recognition*, 2023. 6

DeDoDe: Detect, Don’t Describe — Describe, Don’t Detect for Local Feature Matching

Supplementary Material

In this supplementary material we present implementation details, qualitative examples, and theory that could not fit in the main text.

A. Definitions of Evaluation Metrics

AUC: We evaluate performance using the Area Under the Curve (AUC). We define the $\text{AUC}@t$ as the integral of the precision up to the threshold t . In practice, this is approximated using the trapezoidal rule, as in previous work [8, 29].

Precision: The relative pose estimation precision is defined as

$$\text{Precision}@t = \max(|\varepsilon_{\hat{t}}|, |\varepsilon_{\hat{R}}|) < t \quad (16)$$

where

$$\varepsilon_{\hat{t}} = \arccos \frac{\langle t, \hat{t} \rangle}{\|t\| \cdot \|\hat{t}\|} \quad (17)$$

and

$$\varepsilon_{\hat{R}} = \arccos \left((\text{tr}(\hat{R}^T R) - 1) / 2 \right). \quad (18)$$

Repeatability: First, let

$$\mathbf{x}_{\text{kp} \cap W}^A = \{x_i^A \mid x_i^A \in \text{dom}(W) \cap \mathbf{x}_{\text{kp}}^A\}, \quad (19)$$

where W is the ground truth warp, and its domain $\text{dom}(W)$ are the pixels where it is well defined. In the case of MegaDepth, we will only consider keypoints in the MVS regions. We define repeatability as

$$\frac{1}{|\mathbf{x}_{\text{kp} \cap W}^A|} \sum_{x_i^A \in \mathbf{x}_{\text{kp} \cap W}^A} \left(\min_{x_i^B \in \mathbf{x}_{\text{kp}}^B} \|x_i^B - W(x_i^A)\|_2 \right) < t. \quad (20)$$

In words, this measures the the percentage of keypoints detections in the MVS covisible region with a corresponding keypoint within a certain threshold in the other image.

mAA: For IMC-2022 the performance is measured in mAA, which closely resembles AUC. We further detail the metric below. Given an estimated fundamental matrix, the error is computed in terms of rotation (ε_R in degrees) and translation (ε_T in meters). Given one threshold over each, the pose is classified as accurate if it meets both thresholds. In code:

```
thresholds_r = np.linspace(1, 10, 10) #  
In degrees.  
thresholds_t = np.geomspace(0.2, 5, 10)  
# In meters.
```

The percentage of image pairs that meet every pair of

thresholds is computed, the results are averaged over all thresholds, which rewards more accurate poses. As the dataset contains multiple scenes, which may have a different number of pairs, the metric is computed separately for each scene and then averaged. We refer to this metric as mAA@10.

B. DeDoDe Further Implementation Details

In the following paragraphs, we describe implementation details that did not fit in the main text.

Detector Objective Further Details: We set the prior Uniform constant C such that the peak of the Gaussian centered around the deltas is a factor $\exp(50)$ larger compared to the uniform. In practice, we do these computations in log-space. This ensures that all consistent keypoints are detected, while still allowing the network to detect additional keypoints in cases where the target distribution is overly sparse. We found that the performance of the network was robust to the precise value of C .

Further Detector Architecture Details: For DeDoDe detector dimensionality of the encoded context is [32, 128, 256] for strides [2, 4, 8].

Descriptor Objective Further Details: In addition to enforcing the keypoints to be mutual nearest neighbours, we enforce that the distance be smaller than 0.5% of the image in both directions. We did not find that this had a major impact on performance, possibly due to very few mutual nearest neighbours not fulfilling the criteria.

Descriptor Architecture Further Details: For DeDoDe descriptor-B dimensionality of the encoded context is [32, 128, 256] for strides [2, 4, 8] respectively, for DeDoDe descriptor-G we additionally encode context of dimension 512 for the DINOv2 [22] features at stride 14.

Training Further Details: We use a base learning rate of $2 \cdot 10^{-5}$ for the encoders and $1 \cdot 10^{-4}$ for the decoders. We use a cosine decay learning rate scheduler.

C. Runtime:

Here we measure the runtime of DeDoDe, and compare it to DISK [32]. We run both methods at the inference resolution used in the SotA experiments, which is 1024×1024 for DISK and 784×784 for DeDoDe. We present results in Table 7. We find that DeDoDe has a similar runtime to DISK, and is about $\sim 2.5 \times$ faster for keypoint-only extraction.

	Time (ms)
DeDoDe Det	62.5
DeDoDe Det+Desc-B	103.4
DeDoDe Det+Desc-G	160.0
DISK Det+Desc	170.0

Table 7. **Inference time comparison.** We compare the inference time of DeDode to DISK.

D. Inference Settings for Detector+Descriptors

DeDoDe: We use a resolution of 784×784 . We use a dual-softmax threshold of 0.01.

DISK: We follow the suggested inference approach, and use images of size 1024×1024 , with a NMS radius of 5. We use a dual-softmax matcher with confidence threshold 0.01. We additionally investigated the ratio-test but found it to give inferior results on IMC22.

SiLK: We use the [official settings of SiLK for IMC-2022](#), where the longer side of the image is resized to 720, a dual-softmax matcher with confidence threshold of 0.01, and use 30,000 keypoints. Using this threshold, SiLK produces many outliers, as can be seen in Figure 6. For a fair comparison on MegaDepth-1500 we therefore instead use a threshold of 0.05, which we found beneficial for SiLK.

ALIKED: We find ALIKED to perform the best using a resolution of 800×800 , we sample 10,000 keypoints per image, and use a dual-softmax matcher with confidence threshold of 0.01.

E. Robustness to Large Rotations

We revisit the pair in Figure 5 in a more difficult setting by rotating the first image by 180° . We find that despite not being trained on large rotations, DeDoDe produces good matches. We leave investigations of how to improve performance on non-upright images to future work.

F. Why is top- k Needed?

In Section 4.5 we argued that the top- k thresholding is needed to stabilize training. Here we provide some theoretical reasons why the non-thresholded objective has issues.

To see this, note that the cross-entropy is 0 if and only if $p_{f_\theta} = \delta_{x_i}(x)$, for any x_i . Hence this objective has multiple degenerate solutions. We found that when training, the network collapses into predicting a single peak.

One could instead consider a Kullback-Leibler (KL) divergence between the distributions. This divergence is however also minimized by any $p_{f_\theta} = \delta_{x_i}(x)$.

Stability issues in self-supervised objectives are well-known and many solutions have been proposed, see e.g., Grill et al. [11], Oquab et al. [22].

Our proposed top- k objective is a simple way of avoiding these instabilities. The binarization encourages the network to predict a flat distribution over certain keypoints, ensuring that it does not collapse. The downside of the objective is, as discussed in Section 4.5 that k is an additional hyperparameter that is not obvious how to set optimally and will depend on the dataset.

G. Additional Qualitative Examples

In Figure 9 we provide qualitative examples of DeDoDe on the publically released images of the IMC-2022 benchmark. In Figure 10 we provide an additional example of DeDoDe on the MegaDepth-1500 benchmark.

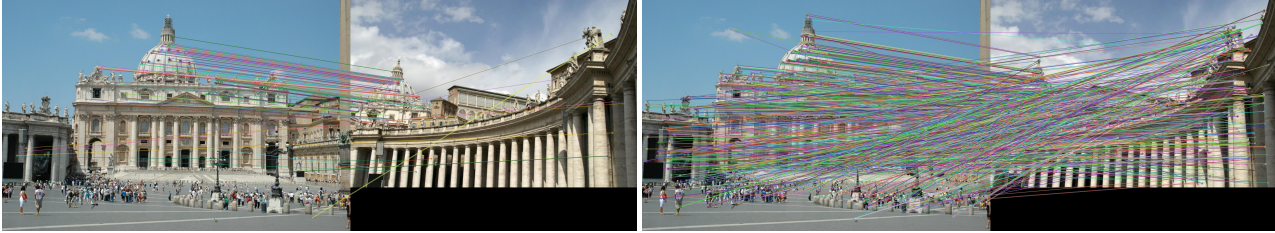


Figure 6. **Issues with SiLK confidence.** At tight confidence thresholds SiLK tends to produce too few but accurate correspondences. However, at looser thresholds a large number of outlier correspondences arise.



Figure 7. **Top-10k Keypoints of DeDoDe.** In contrast to previous methods, our method is able to produce a larger amount of repeatable keypoints, leading to more accurate estimation results. Best viewed in high-resolution.

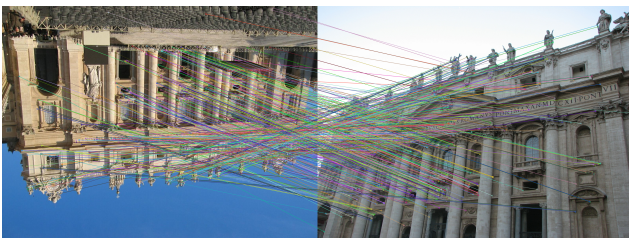


Figure 8. **Robustness of DeDoDe to large rotation.** Despite not being trained on large rotations, and not having an equivariant network architecture, DeDoDe is able to match under even extreme changes in rotation. Rotations do however produce a larger number of outlier correspondences as can be seen in the figure.

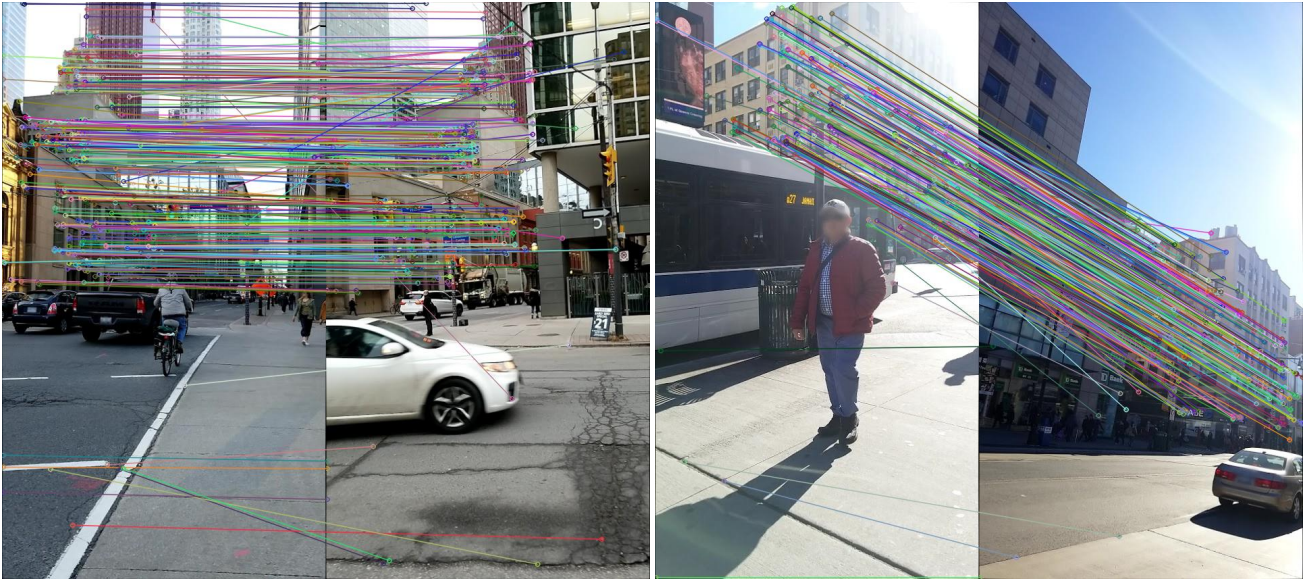


Figure 9. **DeDoDe matches on IMC-2022.** We show matches of two publicly available image pairs from the IMC2022 benchmark.

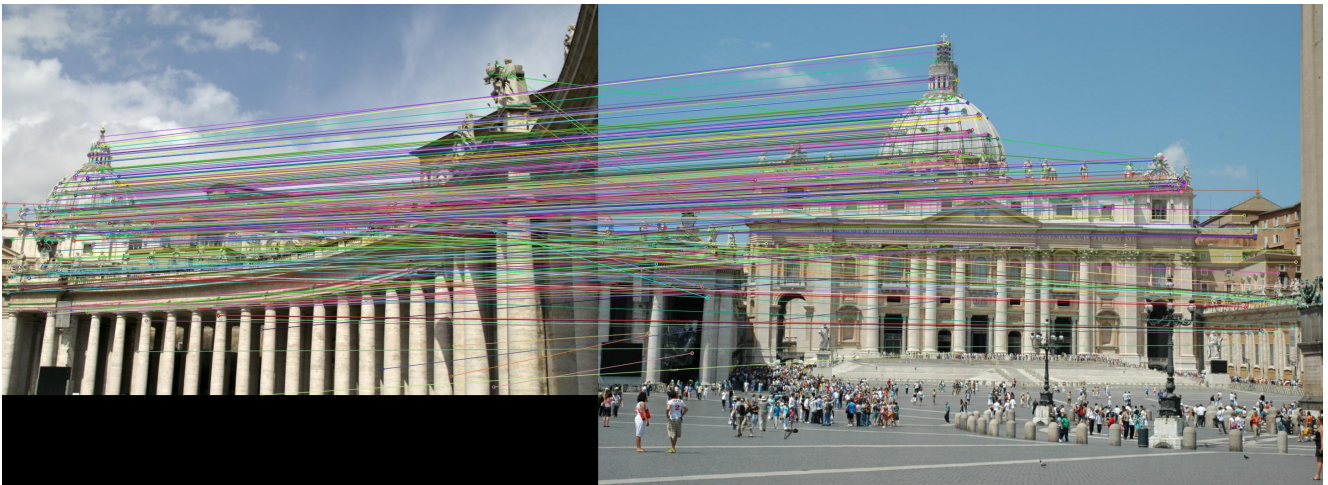


Figure 10. **DeDoDe matches on the MegaDepth-1500 benchmark.**